Bulletin of Earth Sciences of Thailand

THE STUDY OF RESERVOIR DISTRIBUTION AND CONNECTIVITY USING SEISMIC ATTRIBUTES, CENTRAL PATTANI BASIN, GULF OF THAILAND

Nusara Adisaipattanakul*

Department of Geology, Faculty of Science, Chulalongkorn University, Bangkok, 10330, Thailand
*Corresponding author email: nusara.adi@gmail.com

Abstract

Reservoir distribution and connectivity in the Pattani Basin, Gulf of Thailand is always a challenging issue. The reservoirs are relatively thin fluvio-deltaic sands (7-70 ft (2-20 m) on average) and highly compartmentalized by rapid lateral and vertical stratigraphic changes, as well as having an abundance of faults. In order to maximize the production economics, the reservoir connectivity which plays a major role in how the reservoirs are managed and developed must be well understood. This study is aimed to gain a better understanding on reservoir connectivity at 3 sand levels, 3650 ft (1.11 km) (Sand1), 4500 ft (1.37 km) (Sand2) and 7000 ft (2.13 km) (Sand3) true vertical depth sub-sea level (TVDSS). The main 4 possible causes that might result in the not-connected reservoirs among wells are 1) mis-correlated sands, 2) faulted sands 3) internal compartmentalized sands and 4) separated sands. Many seismic attributes were tested to improve fault images. The results of the best fault implication attribute (Variance attribute) showed that there is no major fault amongst well distribution at all 3 sand levels. The sand connectivity study then integrated the Root Mean Square (RMS) amplitude maps that are sand-predictive maps to the well log correlation, pressure data and production-injection data. It revealed that the RMS amplitude can help determine the spatial reservoir distribution, this leads to the more visual reservoir connectivity prediction further to wells without pressure data and/or being perforated. The recommendations for the future sand perforation at Sand1 level and the proposed injector well at Sand3 level have been made to recover the un-swept reserves.

Keywords: Reservoir distribution, Reservoir connectivity, Reservoir compartments, Seismic attributes, Variance attribute, RMS amplitude

1. Introduction

The Pattani Basin is a structurally complex, hydrocarbon prolific rift basin located in the Gulf of Thailand. The basin has been initiated by the northwards movement of the Indian Plate and the subsequent collision with Eurasia Plate in the Eocene (Morley et al. 2011). It was filled by siliciclastic deposits of Tertiary age. The reservoirs are primarily fluvial sandstones to fluvio-deltaic sandstones of Early to Middle Miocene age (Jardine, 1997). The reservoirs are typically thin, 7-70 ft (2-20 m) on average, and they are extremely compartmentalized by rapid lateral and vertical stratigraphic changes. The abundance of normal faults also caused reservoir compartmentalization. As a result, the reservoir connectivity is always a challenging issue for reservoir management and recoveryenhancement.

This study is aimed to gain a better understanding of the reservoir connectivity at 3 reservoir levels; 3650 ft (1.11 km) (Sand1), 4500 ft (1.37 km) (Sand2) and 7000 ft (2.13 km) (Sand3) True Vertical Depth Sub-Sea level (TVDSS) or equivalent to 1.0-1.8 second Two-Way-Time (sec TWT) on Seismic data, in the central part of the Pattani basin. The study integrated the results from seismic attributes analysis to other information including well log data, pressure data and production-injection data.

The seismic amplitude, combined with production data, was previously used to analyze reservoir connectivity in Bohai Bay Oilfield by Libo et al (2016).

2. Methodology

The key steps for this study are 1) rock physics analysis, 2) well-seismic tying, 3) seismic attributes (for fault-horizon interpretation and stratigraphic images) and 4) reservoir connectivity study. The sand connectivity study

integrates the results from seismic attributes to the well log correlation, pressure data and production-injection data. The possible causes that might result in the reservoir dis-connectivity are identified and tested via methods shown in table 1.

3. Observations and Results

3.1 Rock Physics Analysis

In orde to understand the physical properties of sand and shale and their impacts on seismic reflections as the degree of acoustic contrasts, Density, P-wave velocity, S-wave velocity and Acoustic impedance (AI) of well C-04 (the only well that S-wave velocity was acquired) have been plotted against depth (Figure 1). Sand was identified by clay volume less than 0.2 while shale was identified by clay volume greater than 0.6.

The Density Vs Depth plot (Figure 1A) shows that sands have lower density than shales and the separation between sand trend line and shale trend line becomes narrower with depth. The separation of these trend lines are observed through the whole section.

The P-wave velocity Vs Depth plot (Figure 1B) reveals that the P-wave velocity of sands and shales is very similar in the shallow

Possible reasons for sand dis-continuity	Testing methods
1. Mis-correlation (well logs) 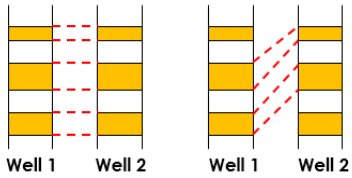	-Sand correlation using well log correlation, fluid type, hydrocarbon contact, pressure data and production-injection data.
2. Faults 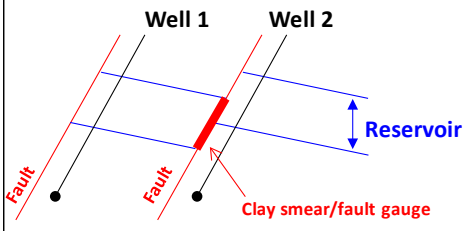	-Seismic attributes 1. Variance/Edge Evidence/Similarity/Smoothed Similarity/ 2. Dip of Max Similarity/Smoothed dip of Max Similarity 3. Instantaneous lateral continuity 4. Most Positive-Most Negative Curvature
3. Internal compartments 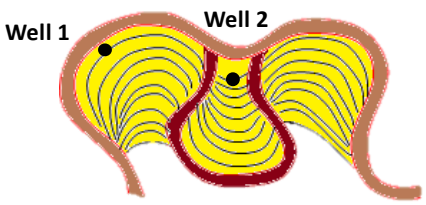	-Seismic attributes 1. RMS/Envelop/Sweetness/Reflector intensity/Relative Acoustic Impedance 2. Shale indicator 3. Spectral Decomposition
4. Different sand bodies 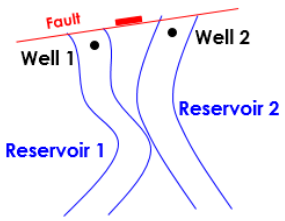	

Table 1 The possible reasons for reservoir dis-connectivity and testing methods.

3. Observations and Results

3.1 Rock Physics Analysis

In order to understand the physical properties of sand and shale and their impacts on seismic reflections as the degree of acoustic contrasts, Density, P-wave velocity, S-wave velocity and Acoustic impedance (AI) of well C-04 (the only well that S-wave velocity was acquired) have been plotted against depth (Figure 1). Sand was identified by clay volume less than 0.2 while shale was identified by clay volume greater than 0.6.

The Density Vs Depth plot (Figure 1A) shows that sands have lower density than shales and the separation between sand trend line and shale trend line becomes narrower with depth. The separation of these trend lines are observed through the whole section.

The P-wave velocity Vs Depth plot (Figure 1B) reveals that the P-wave velocity of sands and shales is very similar in the shallow

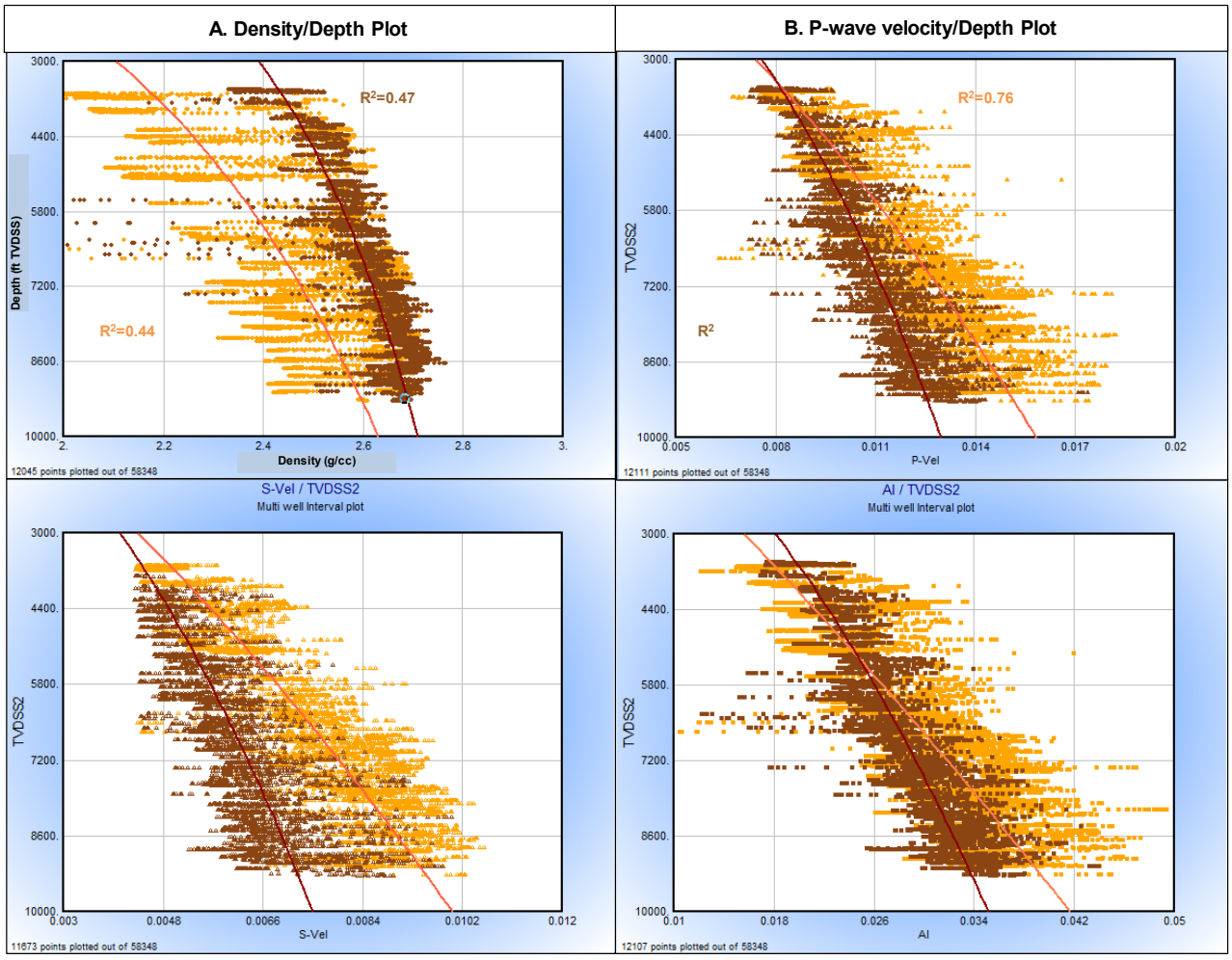

Figure 1 Cross plots of A) Density, B) P-wave velocity, C) S-wave velocity and D) Acoustic impedance (AI) against depth (ft TVDSS) at well C-04. Sand points (clay volume < 0.2) represented by orange color while shale points (clay volume > 0.6) were in brown color. The error ranges of the best fit trend lines (dark orange for sand and dark brown for shale) are shown as R2 values.

section less than 4400 ft TVDSS. Then, sands become faster than shales with increasing depth. The S-wave velocity Vs Depth plot (Figure 1C) shows more separation between sand and shale trend line than P-wave velocity Vs Depth plot.

The AI Vs Depth plot (Figure 1D) shows the crossover of sand trend line and shale trend line at approximate 5,300 ft TVDSS. Sands tend to have lower AI than shales at shallower depth than 5,300 ft TVDSS, then shales become lower AI than sands at deeper depth than 5,300 ft TVDSS.

To conclude, the density and S-wave velocity seem to be able to discriminate sands from shales better than P-wave velocity and Acoustic impedance.

3.2 Well-Seismic Tying

Three wells (C-04, C-13 and D-09) were tied to the 'Supercube' volume, the reprocessed 5-40 degree stack volume, for velocity analysis. First, the wavelets were extracted at well locations in the interval with interest (1.0-2.0 sec TWT). The extracted wavelet shows a dominant frequency at 23 Hz with ringing side-lobes. Based upon the seismic processing report, this volume was processed to be zero-phase which agreed with the water bottom reflection. Consequently, the theoretical Ricker wavelet of zero-phase and 23 Hz dominant frequency was used to create the synthetic traces, by convolving the wavelet with the reflection coefficient that derived from density and the density-based velocity (Gardner's correlation (Gardner et al, 1974). Finally, the synthetic traces were tied to the extracted seismic traces at well locations.

The results from well-seismic tying confirm the phase of seismic data that the increase in AI results in a peak in seismic. The time-depth relations of 3 well-seismic ties and the initial velocity applied prior the tying process, the 'Original velocity', were plotted together. The plot suggests that there is no velocity variation in the study area.

The interval velocities of the original velocity and the 23 Hz dominant frequency were used to calculate the tuning thickness at each reservoir level. The calculated tuning thicknesses at Sand1, Sand2 and Sand3 levels are 95, 105 and 127 ft TVD respectively.

3.3 Seismic attributes

3.3.1 Seismic attributes for fault imaging and reflector continuity enhancement

The original Supercube volume showed some poor fault definitions and highly discontinuous reflectors. Therefore, many seismic attributes were tested to improve the fault imaging and reflector continuity for fault and horizon interpretation.

Firstly, the smoothing attributes, median filter and structural smoothing, were applied to the original Supercube volume. Then, multi-attributes were tested for fault expression by applying the original, median filtered and structural smoothed volumes as inputs.

The results showed that the structural smoothed volume gave the most continuous reflectors with the least lateral amplitude variation. This resulted in the best fault images on the Variance of structural smoothed volume (Figure 2B) which was a large improvement from the original volume (Figure 2A).

Unfortunately, the reflectors in the structural smoothed volume appeared to be thicker than the median filtered and the original volume respectively. In some areas, two reflectors were merged into a single reflector. Moreover, the reflector terminations at faults from the original volume were smeared across faults. Therefore, the median filtered volume was selected for the 3 horizon interpretation at the reservoir levels with interest rather than the structural smoothed volume.

Besides the Variance attribute, the smoothed dip of max similarity (Figure 2D) was thought to be a successful attribute for fault detection as it can illustrate the faults on the NW part of the study area that none of the other tested attributes can. The Curvature attribute was aimed to detect the small-offset faults, one possibility for sand dis-connectivity especially in thin sands. Unfortunately, only some of the major faults corresponded to the most positive curvature values, and the fault imaging is not as clear as the other attributes (Figure 2E).

The same method was done in another set of seismic data that was processed for Amplitude Variation with Offset (AVO) study including full- (0-35 degree), near- (5-22 degree), mid- (18-35 degree) and far- (36-60 degree) angle stack volumes. The result showed that the Variance of structural smoothed near-angle stack volume (Figure 2C) gave the sharpest and most continuous fault images, but some small faults were not as well imaged as the Variance of

structural smoothed Supercube volume.

Finally, the Variance attributes of structural smoothed Supercube at time slices 1.144, 1.320, and 1.768 sec TWT were utilized to express fault distribution at each sand level. There is no major fault indication among the well distribution at each level that could result in a fault-dominated compartmentalized reservoir.

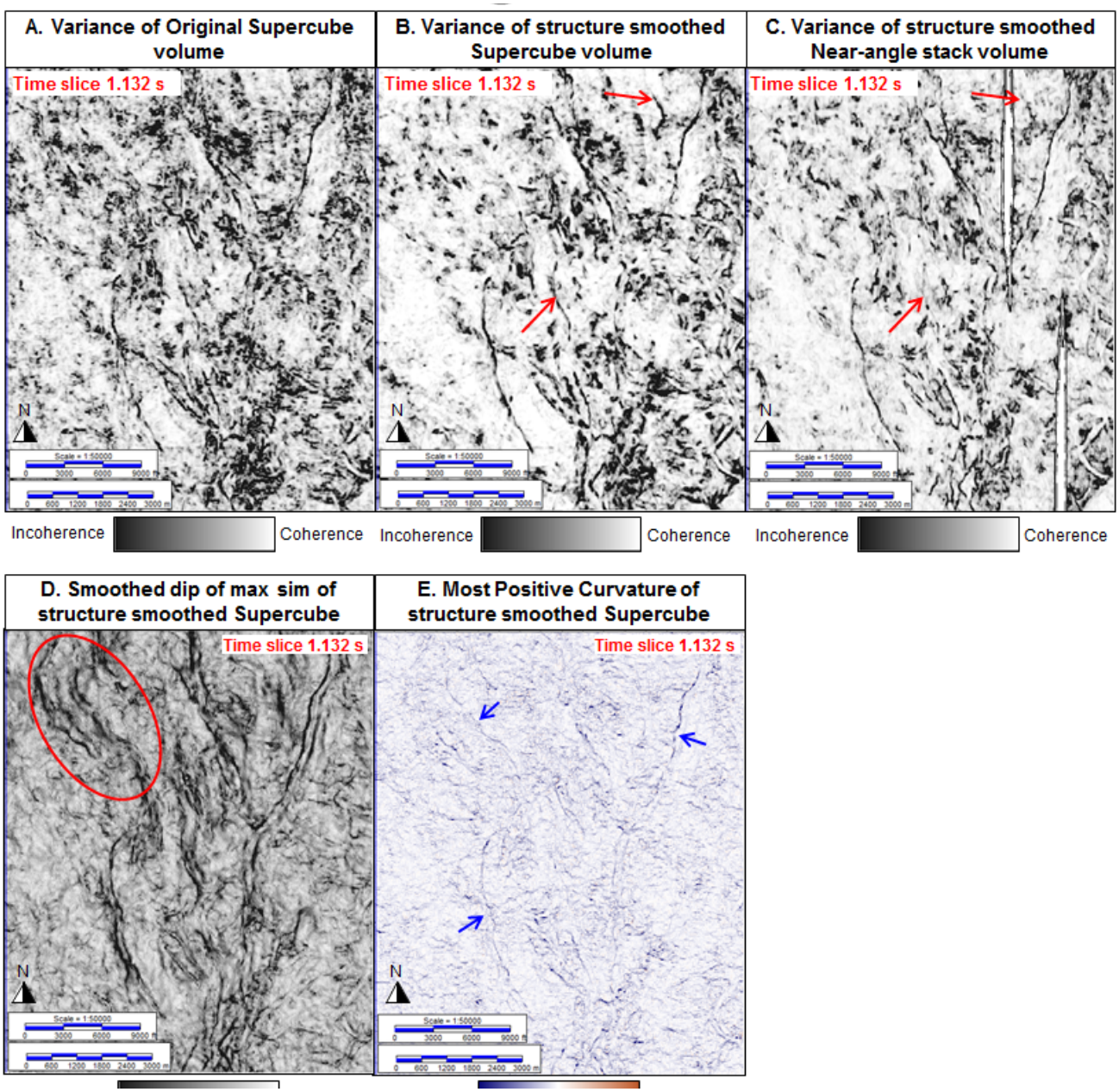

Figure 2 The Variance attributes of the original Supercube (A), structural smoothed Supercube (B) and structural smoothed near-angle stack (C). The fault images in structural smoothed Supercube were highly improved from the original Supercube, and the small faults (red arrows) were better detected than in structural smoothed near-angle stack volume. The Smoothed dip of max similarity of structural smoothed supercube (D) was able to illustrate fault in the NW part of study area. The Most positive Curvature (E) expressed some major faults (blue arrows).

3.3.2 Seismic attributes for Stratigraphic feature visualization

The RMS amplitude at each sand level was extracted along the horizon within the window that cover the shale above and below the sand interval. The extraction was done in all volumes; Supercube, full-, near-, mid- and far-angle stack volume.

The results suggested that the RMS amplitude map extracted from the Supercube volume is the best Sand-predictive map, and the changes of RMS amplitude via increasing incident angle of partial-angle stack volumes can help fluid identification. For example, the hydrocarbon-bearing sand at well C-09, C-12 and C-14 showed high RMS amplitude on far-angle stack but low amplitude on near- and mid-angle stack. The wet sand at well C-11 showed high amplitude on near- and mid-angle stack but became dim on far-angle stack (Figure 3).

The spectral decomposition is aimed to improve the imaging of thin reservoirs and test the ability of sand thickness prediction by applying the higher frequency than the actual dominant frequency (23 Hz) to the seismic data, then, the RMS amplitude is extracted from each frequency of spectral decomposed volumes. This is due to the fact that the seismic amplitude will be highest when the sand thickness is equal to the tuning thickness, which is thicker than the actual sand thickness.

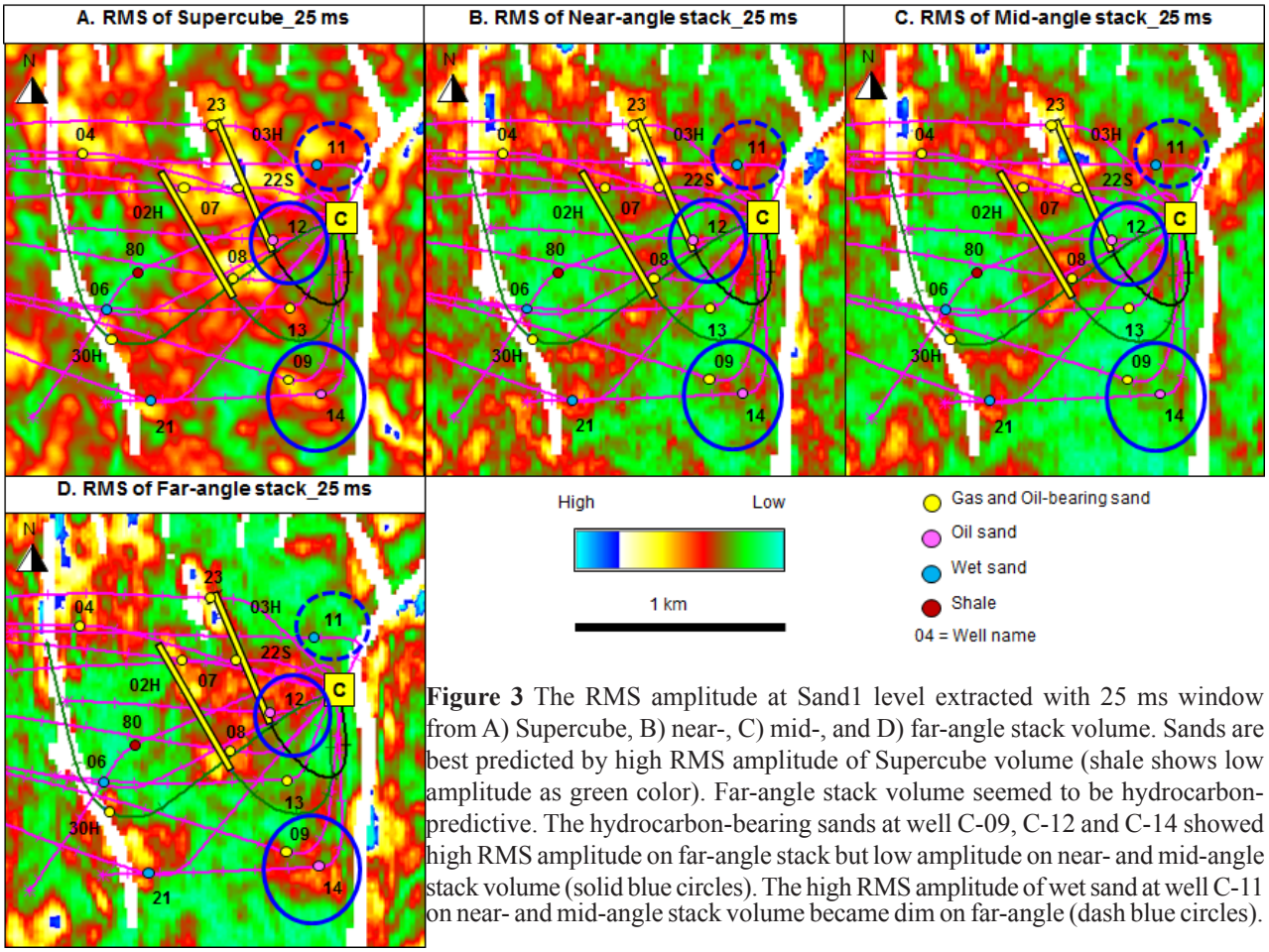

Figure 3 The RMS amplitude at Sand1 level extracted with 25 ms window from A) Supercube, B) near-, C) mid-, and D) far-angle stack volume. Sands are best predicted by high RMS amplitude of Supercube volume (shale shows low amplitude as green color). Far-angle stack volume seemed to be hydrocarbon-predictive. The hydrocarbon-bearing sands at well C-09, C-12 and C-14 showed high RMS amplitude on far-angle stack but low amplitude on near- and mid-angle stack volume (solid blue circles). The high RMS amplitude of wet sand at well C-11 on near- and mid-angle stack volume became dim on far-angle (dash blue circles).

The results showed that all sand thickness ranges showed highest amplitude on the RMS amplitude map extracted from 26 Hz-spectral decomposed volume, which is more or less the dominant frequency. This is possibly the result of the insufficient high-frequency data on the seismic data.

Amplitude attributes including RMS, Envelop, Sweetness, and Reflector intensity were created from the Supercube volume and displayed on the stratal slice, the flattened seismic dataset with reference to a horizon (Zeng et al, 1998a; Zeng et al, 1998b; Van dyke, 2006; Zeng, 2010; Van dyke, 2015), at each of the reservoir level with interest. These attributes were then compared to the RMS amplitude extracted from the horizon.

The high amplitude distribution of all attributes and the extracted RMS amplitude are quite consistent. Therefore, the RMS amplitude extracted from the horizon was considered as a representative map for reservoir imaging and was further utilized for reservoir connectivity study.

3.4 Sand Connectivity

3.4.1 Sand1 level (approx. 3650 ft TVDSS)

The sand correlation based on the log characters suggested that this gas-oil reservoir possibly extends through all 12 wells, the thickness varies from 22-80 ft TVD thick. This is likely to be the amalgamated fluvial sands rather than one-single sand as the common range of fluvial sand thickness is 13-65 ft (4-20 m) (Gibling, 2006).

The horizontal sections of C-02H and C-03H, the production test and the injection result confirmed that sand connectivity of 6 wells; C-23, C-03H, C-22S, C-07, C-02H and C-08. The log characters and the extensive seismic amplitude anomaly at RMS amplitude map extracted from Supercube volume with 25 ms window at Sand1 level (Figure 4A) suggested that this sand is likely connected through C-12 and C-13, and possibly connected with C-04 and C-30H. However, this extensive anomaly is totally separated from the high amplitude body at C-09 and C-14 by the low amplitude area (green color). This indicates at least 2 separated reservoirs at Sand1 level that was supported by the inconsistent gas-oil contact of C-09 (3701 ft TVDSS) with other wells (3671-3681 ft TVDSS).

3.4.2 Sand2 level (approx. 4500 ft TVDSS)

The sand correlation based on the log characters suggested that this gas-oil reservoir possibly extends through 7 wells with thickness range of 22-58 ft TVD.

The RMS amplitude map extracted from Supercube volume with 20 ms window at Sand2 level (Figure 4B) suggested that the hydrocarbon-bearing sand at C-09, C-54H, B-32H and B-16 are likely to be connected but probably separated from other wells by the low RMS amplitude area as non-reservoir. The RFT of C-80 (tested in January 2012) suggested a depleted reservoir that is probably connected to C-06 which is the nearest producing well (started producing in August 2005).

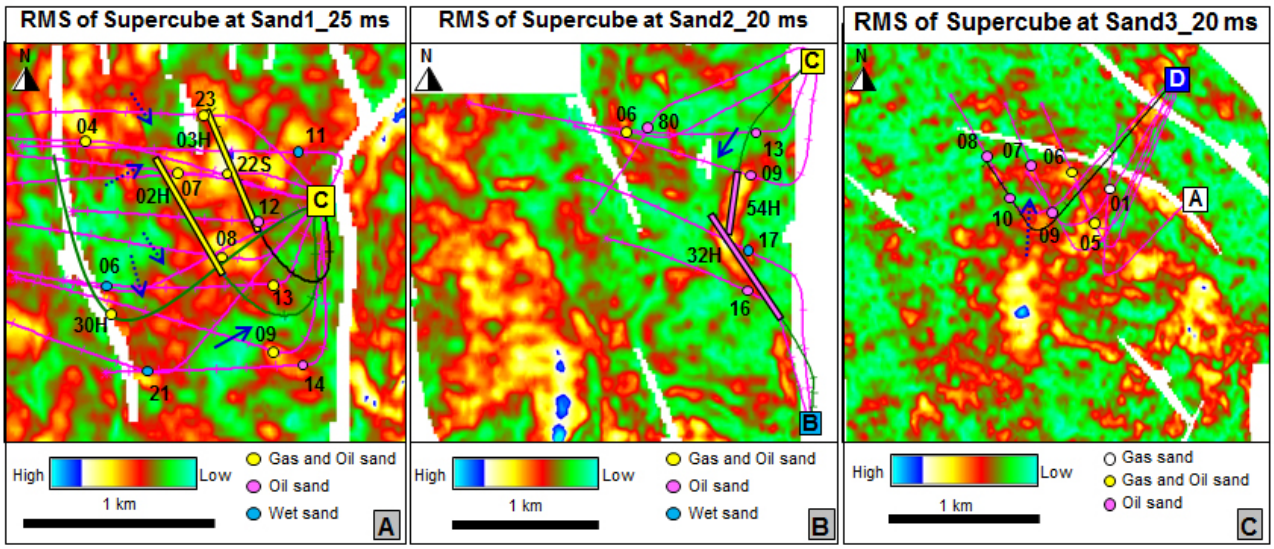

Figure 4 The RMS amplitude extracted from Supercube at A) Sand1 level with 25 ms window, B) Sand2 level with 20 ms window and C) Sand3 level with 20 ms window. The solid blue arrows point to the low amplitude area that totally and partially separate high amplitude bodies, and dashed, respectively. At Sand1 level, C-09 and C-14 is likely to be isolated from the other wells. At Sand3 level, the connectivity along D-07, D-06, A-01 and D-05 should be better than the others.

3.4.3 Sand3 level (approx. 7000 ft TVDSS)

The sand correlation based on the log characters suggested that this gas-oil reservoir possibly extends through 7 wells with thickness range of 22-54 ft TVD.

The production test suggested the possible pressure communication of the injector well (D-10) and the nearby producing well (D-07, D-09 and D-05). However, the production-injection data did not show a significant increase in production rate after water injection. This might be due to the lateral-permeability barrier that could prevent fluid flow as seen in well log as a shale break within the sand interval of well D-08, D-10 and D-07.

The RMS amplitude map extracted from Supercube volume with 20 ms window at Sand3 level (Figure 4C) showed low amplitude patches (green color) among well distribution and particularly at the injector well (D-10). This suggested that the reservoir quality might not be as good as the extensive, continuous, high amplitude anomaly observed at Sand1 level. The high amplitude at Sand3 level extends more continuously through D-07, D-06, A-01 and D-05, so it is believed that the connectivity among these wells should be better than others.

4. Discussions and Recommendations

The 3 main topics from this study are summarized below;

1. Lithology discriminator from rock physics analysis.

The rock physics analysis showed that the density and S-wave velocity are able to discriminate sand from shale better than P-wave velocity and the acoustic impedance. The S-wave velocity in liquid median equals zero, hence, it eliminates the fluid effects and emphasizes the matrix properties.

The density-, the S-wave velocity-, and the elastic impedance (EI) inversion volume might be the better starting volumes for reservoir characterization than the acoustic impedance volume. This is recommended for further study.

2. Reservoir and hydrocarbon implications using multi-seismic volumes.

The RMS amplitude extraction from multi-seismic volumes suggested that the RMS map of Supercube volume is the best map for sand prediction and, in some cases, the changes of amplitude distribution with incident angle of partial-angle stack volumes can also help determine fluids. Some hydrocarbon-bearing sands show high amplitude at only far-angle stack volumes, and low amplitude at near- and mid- angle stack volumes. On the contrary, the wet sands that show high amplitude at near- and mid-angle stack volume become dim at far-angle stack volume. This is considered as an AVO (Amplitude Variation with Offset) effects on hydrocarbon bearing sands. The far incident angle (> 30 degree) could increase the P-wave velocity difference of HC-bearing sand and shale (third term of Shuey's equation (Shuey, 1985)) which results in the greater reflection coefficient. Integration of Supercube RMS map for reservoir identification and the Far-angle stack RMS map for fluid identification might be helpful for well location selection.

1. RMS Amplitude maps application for spatial reservoir connectivity The distribution of high RMS amplitude of Supercube volume is used to support and guide the reservoir connectivity interpretation between wells. The high amplitude represents sand and the low amplitude indicates non-reservoir (shale). The extensive, high amplitude anomaly observed at Sand1 level suggested a good connectivity between wells. On the contrary, the area where many low amplitude patches are observed, such as at Sand3 level, is likely to have poorer connectivity. By gaining better understanding on the reservoir connectivity, recommendations have been made to recover the un-swept reserves as followed; 1) perforate the hydro-carbon bearing sand at either C-09 or C-14 (non-perforated reservoir) which is likely isolated from the producing wells (C-23,C-02H and C-03H) at Sand1 level, 2) D-07 is the best injector candidate for future water-flooding as it is likely to connect with the more updip producing sand of D-07, D-06 and D-05.

5. Conclusions

The key findings and conclusions are listed below;

1. The density and S-wave velocity can be used as lithology discriminators better than P-wave velocity and acoustic impedance.
2. The Structural smoothing attribute can clean up the seismic data, by improving the reflector continuity and enhancing the edges, which results in the better fault images.
3. The Variance attribute and (Smoothed) Dip of Maximum similarity attributes are very useful for fault illustration, especially those of structural smoothed Supercube.
4. The RMS amplitude map extracted from the Supercube volume is the best sand-predictive map. The RMS amplitude map extracted from the far-angle stack volume is helpful for fluid identification (non-hydrocarbon or hydrocarbon).
5. Sand1 level could have at least 2 reservoirs. First reservoir extends through C-23, C-03H, C-22S, C-07, C-02H, C-08 (certainly), C-12, C-13 (probably), C-04 and C-30H (possibly). The second reservoir covers well C-09 and C-14. Future perforation at the second reservoir (non-perforated) is recommended.
6. Sand2 level could have at least 2 reservoirs. First is C-06 and C-80 (probably), second is C-09, C-54H, B-32H, B-16 (probably) and C-13 (possibly).
7. Sand3 level shows possible pressure-communication of well D-10, D-07 and
8. D-09. It seems to have high lateral permeability barrier adjacent to injector well (D-10) which could prevent fluid flow and resulted in no significant hydrocarbon production response from injection. D-07 is recommended to be an injector candidate for future water-flooding as the sand connectivity along D-07, D-06, A-01 and D-05 is believed to be better than other wells.

6. Acknowledgements

Firstly, I would like to express my deeply gratefulness to my research advisor, Professor Angus Ferguson, for his comfortable guidance, persistent encouragement, as well as his very helpful suggestions and comments during my research period. Secondly, I would like to thank Chevron Thailand E&P for the use of their data. I would also express my recognition to Ms. Nualjun Kitvarayut, the Geology Technical Manager, who allowed this project to be possible, and Mr. Kenneth Lewis, a senior earth scientist at Reservoir Management Department, who brought up this challenging issue and led to this research topic, Mr. Nuttapong Keawmoon, and all of my co-workers and my colleges for the good discussions. Finally, I must express my profound gratitude to my parents for their persistent support and encouragement.

7. References

Gardner, G. H. F., Gardner, L. W., and Gregory, A. R., 1974, Formation Velocity and Density-the Diagnostic Basics for Stratigraphic Traps, Geophysics, v. 39, p. 770-780.

Gibling, M. R., 2006, Width and thickness of fluvial channel bodies and valley fills in the geological record: A literature compilation and classification: Journal of Sedimentary Research, v. 76, p. 731–770.

Jardine, E., 1997, Dual Petroleum Systems Governing The Prolific Pattani Basin Offshore Thailand, Proceedings of the International Conference on Petroleum Systems of SE Asia and Australasia Conference, May 1997, p. 351-363.

Libo, G., Feng, Z., Yuzhen, W., and Jungang, W., 2016, Analyse on Reservoir Connectivity Constrainted by Seismic Data, SPG/SEG Beijing 2016 International Geophysical Conference.

Morley, C. K., Charusiri, P., and Watkinson, I. M., 2011, Structural geology of Thailand during the Cenozoic, In: Ridd, M. F., Barber,

A. J., and Crow, M. J. (eds) The Geology of Thailand: Geological Society of London, p. 273-334.

Shuey, R. T., 1985, A simplification of the Zoeppritz equations, Geophysics, v. 50, no. 4, p. 609-614.

Van Dyke, S. K., 2006, Geoscientific Workflow Process in Drilling a Deepwater Well, Offshore Morocco, In: Annual Bob F. Perkins Research Conference Proceedings, 2006. GCSSEPM Foundation, p. 1233-1256.

Van Dyke, S. K., 2015, Stratal Slicing, An Application for Seismic Sedimentology, International Basic and Applied Research Journal, v. 1, p. 1-6.

Zeng, H., 2010, Stratal Slicing: benefits and challenges, The Leading Edge, v. 29, p. 1040–1047.

Zeng, H., Backus, M. M., Barrow, K. T., and Tyler, N., 1998a, Stratal Slicing, Part I: Realistic 3-D Seismic Model. Geophysics, v. 63, p. 502–513.

Zeng, H., Henry, S. C., and Riola, J. P., 1998b, Stratal Slicing, Part II: Real Seismic Data. Geophysics, v. 63, p. 514–522.